International Journal of Biological Macromolecules 57 (2013) 174–184

Contents lists available at SciVerse ScienceDirect

International Journal of Biological Macromolecules

journal homepage: www.elsevier.com/locate/ijbiomac

Characterization of *N*-trimethyl chitosan/alginate complexes and curcumin release

Alessandro F. Martins*, Pedro V.A. Bueno, Elizângela A.M.S. Almeida, Francisco H.A. Rodrigues, Adley F. Rubira, Edvani C. Muniz

Grupo de Materiais Poliméricos e Compósitos, GMPC – Departamento de Química, Universidade Estadual de Maringá – UEM, Av. Colombo 5790 – CEP 87020-900, Maringá, Paraná, Brazil

ARTICLE INFO

Article history:
Received 27 December 2012
Received in revised form 30 January 2013
Accepted 9 March 2013
Available online 16 March 2013

Keywords:
N-trimethyl chitosan
Sodium alginate
Polyelectrolyte complex
Curcumin
Controlled release
Beads

ABSTRACT

N-trimethyl chitosan of two quaternization degrees, DQ = 20 and 80 mol% and labeled as TMC20 and TMC80, were synthesized and characterized by ^{1}H NMR. Polyelectrolyte complexes (PECs) of TMC/alginate (TMC/ALG) were prepared at pHs 2, 7 and 10 by mixing the aqueous solutions of unlike polymers. The PECs were characterized through infrared spectroscopy (FTIR), thermogravimetric analysis (TGA/DTG) and wide-angle X-ray scattering (WAXS). Using the TMC of DQ = 20 mol% and following the same methodology for preparing the PECs, beads of TMC20/ALG were obtained at pH 2 and loaded with curcumin (CUR) at pH 6.0–6.5. The morphology of the beads was evaluated by scanning electron microscopy (SEM). Studies *in vitro* of the controlled release of CUR from beads were investigated in simulated intestinal fluid (SIF) and simulated gastric fluid (SGF) and treated using conventional and partition-diffusion models. Results indicated that the beads based on TMC20 and ALG presented potential as drug-carrier to improve the solubility and biological activity of CUR at pH close to physiological one.

1. Introduction

Chitosans (CHT) are deacetylated derivatives of chitin, composed by β-(1,4)-2-amino-2-deoxy-D-glucopyranose units and small amount of *N*-acetyl-D-glucosamine residues [1]. CHT owns interesting properties including antimicrobial activity, biocompatibility, biodegradability, low toxicity, mucoadhesivity and accelerating wound healing [2], among others. However, the low solubility of CHT in neutral and alkaline media limits its use in some potential applications, especially for delivering drugs in gastrointestinal tract environments [3]. Therefore, studies turned to the *N*-trimethyl chitosan (TMC), a partially quaternized derivative of CHT, that present solubility at wide range of pH and, therefore, overcomes the solubility limitations presented by CHT at neutral and basic conditions. It also has been shown that TMC can decrease the transepithelial electrical resistance (TEER) of Caco-2 cell monolayers and increase the transport of several hydrophilic compounds, peptide and protein drugs both *in vitro* (Caco-2 cells) and *in vivo* (rats and pigs) [4–6]. So, the TMC has received considerable attention in drug and gene delivery not only in peroral route [7], but also in ocular [8], intranasal [9], buccal [10], pulmonary [11] and rectal routes [12]. Therefore, due to the good solubility of TMC, several studies were reported in the literature in recent years. The main interest of many researchers is to replace the CHT by TMC in the matrix of polyelectrolyte complexes. This fact makes itself interesting and advantageous due to maintenance of the properties of biodegradability, biocompatibility, mucoadhesivity and low toxicity by part of TMC. Also, the TMC presents elevated bactericidal activity as compared to the CHT. Therefore, TMC is a well-studied quaternary CHT derivative that is promising for various pharmaceutical applications [13,14].

Polyelectrolyte complexes (PECs) of *N*-trimethyl chitosan/heparin (TMC/HP) were previously prepared and characterized in our group [15,16]. Studies have confirmed that the PEC of TMC/HP obtained in alkaline medium (pH 8) presented potential to release HP in intestinal conditions (pH 7.4). Nanoparticles of TMC presented excellent property of mucoadhesion and potential for oral delivery of vaccine [17], insulin [18], cisplatin [19], DNA [20] and peptides/proteins [6,21].

Sodium alginate (ALG) is an anionic polysaccharide obtained from marine algae. The ALG is a water-soluble natural copolymer composed of guluronic acid and mannuronic acid units. This biopolymer has been used as vehicles for delivering various protein drugs because of its biodegradable and biocompatible properties as well as excellent characteristics for maintaining the bioactivity

* Corresponding author. Tel.: +55 44 3011 3676; fax: +55 44 3011 4125.
E-mail address: afmartins50@yahoo.com.br (A.F. Martins).

0141-8130
http://dx.doi.org/10.1016/j.ijbiomac.2013.03.029

of the proteins [22,23]. In addition, the ALG also has been used in pharmaceutical formulations as antiulcer agent, antacid agent and wound protectant. Calcium alginate beads are frequently used as hydrogel due to their innocuousness and ease for gel forming and reported for biomedical applications [22,24,25].

Curcumin (1,7-bis-(4-hydroxy-3-methoxy-phenyl)-hepta-1,6-diene-3,5-dione, is a natural pigment derived from an active component of *Curcuma longa*. Studies suggest that curcumin (CUR) has potential as antimicrobial [26], antiviral [27], anticancer [28] and wound healing activities [29]. However, the hydrophobic feature of CUR inhibits, for instance, its vascular and oral administration due to its barely solubility in water. One alternative to overcome this limitation is to deliver the CUR through some release device (hydrogels, beads and particles, for instance). The employment of such systems in controlled drug delivery has been widely explored [30]. So, the purposes of this work were prepare polyelectrolyte complexes (PECs) of N-trimethyl chitosan/alginate (TMC/ALG) at different pH, employing TMC of low (DQ = 20 mol%) and high quaternization degree (DQ = 80 mol%) and characterize the PECs through FTIR, TGA/DTG, WAXS and SEM. Other target of this work was to perform *in vitro* studies of controlled release of CUR in simulated intestinal fluid (SIF) and simulated gastric fluid (SGF). It is worth to highlight that the formation, characterization and application of PECs (based on TMC and ALG) as a potential carrier to improve both the solubility and the biological activity of CUR were not discussed in the literature yet.

2. Materials and methods

2.1. Materials

Chitosan (CHT, CAS 9012-76-4), with deacetylation degree 85 mol% and M_V 87×10^3 g mol^{-1}, was purchased from Golden-Shell Biochemical (China). Sodium alginate (ALG, CAS 9005-38-3) was purchased from Across Organics (New Jersey, USA) and the ratio of mannuronic acid to guluronic acid (M/G) of the alginate is 1.56, according to the manufacturer. It has already been reported [31] that the values of the average number (M_n) and average-weight (M_w) molecular weights for this alginate are 339,000 and 1,073,000 g mol^{-1}, respectively. Methyl iodide (CAS 74-88-4); *N*-methyl-2-pyrrolidinone (NMP, CAS 872-50-4) and curcumin from *Curcuma longa* (Turmeric) (CAS 458-37-7) were purchased from Sigma–Aldrich (USA). Other reactants such as sodium hydroxide, sodium iodide, sodium chloride, hydrochloric acid, ethanol and diethyl ether, also utilized in this work, were of analytical grade. All reactants were used as received without some further purification step.

2.2. Methods

2.2.1. Synthesis of TMC

As mentioned, TMC wit different degree of quaternization (DQ = 80 and DQ = 20 mol%) were synthesized. The labels TMC20 and TMC80 were used for correlating the DQ of each synthesized TMC.

For obtaining TMC20 a one-stepped reaction methodology was used. For this, 10 g of CHT were previously weighed and dissolved in 400 mL of *N*-methyl-2-pyrrolidinone (NMP) at 45 °C for c.a. 30 min. Then, 24 g of NaI and 60 mL of aqueous NaOH 15% w/v were added to the reaction medium, maintaining the magnetic stirring for 20 min. After keeping the system under reflux, 55 mL of methyl iodide were added and the reaction proceeded for 1 h at 45 °C. The product, *N*-trimethyl chitosan iodide (TMC), was collected after precipitation utilizing ethanol (300 mL to each 100 mL of solution). Therefore, the precipitate was separated by centrifugation (3000 rpm for 5 min), washed with ethanol (four times) and diethyl ether (three times), filtered and dried under vacuum at 40 °C for 48 h. Finally, the product TMC was dissolved in aqueous sodium chloride solution at 10% w/v for exchange iodide ions to chloride ones. Then, the *N*-trimethyl chitosan chloride (TMC) was precipitated in ethanol and finally isolated by centrifugation, following the same methodology as described for the TMI purification. The product was stored in a dark compartment for preparation and characterization of PEC TMC20/ALG.

For the synthesis of TMC80 a two-stepped reaction methodology was employed. It was previously reported by Sieval et al. [32]. The iodide-TMC20 obtained as earlier described was precipitated with ethanol and isolated by centrifugation. After being washed with ethanol and ether, the product was filtered and dried under reduced pressure. This TMC was further dissolved in NMP under constant stirring. Sodium iodide, aqueous sodium hydroxide solution, and methyl iodide were added with rapid stirring. Afterwards, methyl iodide and sodium hydroxide pellets were added and the stirring was continued for 1 h. The product was precipitated in ethanol and washed with ether, filtered, and dried under reduced pressure. In a sequence, the product was dissolved in 10% (w/v) sodium chloride solution for iodide ionic exchange. Then, the TMC obtained was precipitated in ethanol and finally isolated by centrifugation. The product was stored in a dark compartment for preparation and characterization of PEC TMC80/ALG.

2.2.2. Measure of intrinsic viscosity of TMC20 and TMC80

The intrinsic viscosities of the TMC20 and TMC80 in buffer acetic acid/sodium acetate solution were measured according with the methodology described by Follmann et al. [33]. The experiments were performed using an Ubbelohde-type capillary viscometer (Model Cannon 100/E534) at 25 °C. The obtained values of M_V were 26×10^3 g mol^{-1} for TMC20 and 13×10^3 g mol^{-1} for TMC80. The Mark–Houwink–Sakurada constants used for TMC with an acetylating degree of 15 mol% were $K = 1.38 \times 10^{-5}$ and $a = 0.85$ [33].

2.2.3. Preparation of polyelectrolytes complexes (PECs) of TMC/ALG

The PECs were formed at different conditions (pH 2, 7 and 10) while the volume ratio TMC-solution to ALG-solution was kept constant. The following procedure was adopted: aqueous solutions of TMC20 or TMC80 (2.0 g in 200 mL of distilled water) and ALG (0.5 g in 100 mL of distilled water) were prepared. The TMC-solution (TMC20 or TMC80, 1.0% w/v) was split in five aliquots of 40 mL. The pH of each aliquot was adjusted to a desired value (2, 7 or 10) by adding aqueous solution of HCl and/or of NaOH (0.10 and 1.0 mol L^{-1}). The pH of ALG-solution was also adjusted with NaOH and/or HCl aqueous solutions. The TMC-solution and ALG-solution showed clear, except for the ALG solution prepared at pH 2, which presented slight opalescence. Afterwards, 20 mL of a previously prepared ALG-solution (0.5%, w/v), at desired pH (2, 7 or 10) were slowly dropped into a respective TMC-solutions aliquot (TMC20 or TMC80), at room temperature and under magnetic stirring, keeping the volume ratio at 1/2 (ALG-solution/TMC-solution). The PECs of TMC20/ALG (prepared at pH 7 and 10) and PECs of TMC80/ALG (formed at pH 2, 7 and 10) were obtained in precipitated form. The precipitated material was separated by filtration and, then, frozen and lyophilized at −55 °C for 48 h.

Only the PEC of TMC20/ALG prepared at pH 2 was obtained in the form of beads. Acetone (c.a. 5 mL) were dropped into suspension (60 mL) containing the beads. The suspension was slowly stirred and allowed to stand for c.a. 5 min, until complete decantation of the beads and then 15 mL of supernatant were removed. This process was repeated two times and, thus, volume of solution was reduced to c.a. 30 mL and the water content inside beads diminished substantially. Thus, the beads presented consistence

and the liquid phase, composed by water and acetone, was easily removed from the suspension. This process avoided the collapsing of beads. The beads were washed with 20 mL of a solution of distilled water/acetone 1/1 (v/v). Then, the beads were transferred to polystyrene Petry dish and manually separated from each other. The drying of beads was performed at room temperature (c.a. 25 °C) during 96 h.

The PECs of TMC20/ALG prepared at pHs 7 and 10 were labeled as PEC1 and PEC2, while the PECs of TMC80/ALG prepared at pHs 2, 7 and 10 were labeled as PEC3, PEC4 and PEC5, respectively. The beads of TMC20/ALG prepared at pH 2 were referred in this work as BEADS.

2.3. Characterization

2.3.1. NMR measurements

^{1}H NMR spectra were performed on a Varian, Mercury Plus 300 BB NMR spectrometer, operating at 300.06 MHz for ^{1}H frequency. For acquisition of ^{1}H NMR spectra, 10 mg of CHT were dissolved in 1.0 mL of D_2O/HCl (100/1, v/v) and 10 mg of TMC20 or TMC80 were dissolved in 1.0 mL of D_2O. The ^{1}H NMR spectra were acquired at room temperature and the main acquisition parameters were as follows: pulse of 45°; recycle delay of 10 s and acquisition of 128 transients. Time-domain data were apodized with a 0.2 Hz exponential function (lb) to improve the signal-to-noise ratio before Fourier transformation.

The DQ of the TMC20 and of the TMC80 were determined through the sum of the ratios between the areas of the signals: (i) due to the hydrogen of methyl groups pertaining to acetamide moieties [$NHCOCH_3$], (ii) due to the hydrogen of methyl groups of the dimethylated sites [$(CH_3)_2$], and (iii) due to the methyl hydrogen of the quaternized [$(CH_3)_3$] sites, to the respective number of hydrogen atoms in the each group. Eqs (1) and (2) were used for DQ determination from ^{1}H NMR spectrum of TMC [3,15,34].

$$S = \left[\frac{(CH_3)_3}{9}\right] + \left[\frac{(CH_3)_2}{6}\right] + \left[\frac{NHCOCH_3}{3}\right] \quad (1)$$

$$DQ\% = \left[\frac{(CH_3)_3}{9} \times \frac{1}{s}\right] \quad (2)$$

2.3.2. FTIR spectroscopy

FTIR was used to characterize the chemical structure of materials (ALG and PECs). In each case, KBr disc with 1.0 wt% of sample was prepared. The equipment from Shimadzu Scientific Instruments (Model 8300, Japan) was used at the following conditions: range of 4000–500 cm^{-1}, resolution of 4 cm^{-1} obtained after cumulating 64 scans.

2.3.3. Thermal analysis through TGA and DSC

TGA/DTG analyses of materials were carried out on a thermogravimetric analyzer (Netzsch, model STA 409 PG/4/G Luxx, USA) at a rate of 10 °C min^{-1} under nitrogen atmosphere flowing at 20 mL min^{-1} at temperature range from 30 to 550 °C. DSC analysis were performed on a calorimeter (Netzsch, model STA 409 PG/4/G Luxx, USA) operating at the following conditions: heating rate of 10 °C min^{-1}, nitrogen flow rate of 50 mL min^{-1}, temperature range from 40 to 210 °C.

2.3.4. Scanning electron microscopy (SEM)

The morphology of BEADS was investigated through SEM images (Shimadzu, model SS 550). BEADS surfaces were sputter-coated with a thin layer of gold for SEM visualization. The SEM images were taken by applying an electron accelerating voltage of 15 kV.

2.3.5. Wide angle X-ray scattering (WAXS)

The WAXS profiles were recorded on a diffractometer Shimadzu model XRD-600 equipped with a Ni-filtered Cu-K_α radiation. The WAXS profiles were collected in a scattering range of 2θ = 5–70°, with resolution of 0.02°, at a scanning speed of 2° min^{-1}. The analyses were performed by applying an accelerating voltage of 40 kV and a current intensity of 30 mA.

2.4. Loading of curcumin (CUR) into TMC/ALG BEADS

For loading CUR into the TMC/ALG BEADS, 1.0 mg of CUR was solubilized in 100 mL of water/THF solution (1:1, v/v) at pH 6.0–6.5 and then c.a. 1.0 g of BEADS was transferred to that solution. The system BEADS/CUR solution was kept under magnetic stirring for 24 h at room temperature. So, the BEADS were easily separated by decantation and the supernatant was analyzed through UV-Vis spectroscopy for estimating the loading efficiency [35]. The supernatant was analyzed at 430 nm using a UV-Vis spectrometer (Femto, model 800Xi, Brazil). The analytical curve (R^2 = 0.999) was built from standard CUR solutions with conc. varying from 0.10 to 10 mg L^{-1} using water/THF solution (1:1) as solvent.

2.5. In vitro curcumin release

The *in vitro* CUR release studies were performed in two different environments, both without the presence of enzymes: simulated intestinal fluid (SIF, 6.80 g of KH_2PO_4 and 77 mL aqueous NaOH 0.20 mol L^{-1} in 1000 mL of water, pH = 6.8); and simulated gastric fluid (SGF, 2.0 g NaCl and 7.0 mL of concentrated aqueous solution of HCl 37% (v/v) in 1000 mL of water, pH = 1.2). The releasing studies were carried out in a dissolutor apparatus. For each run, 200 mg of dried and loaded BEADS were deposited in a sealed flask with 150 mL of SIF or SGF. For each condition, the release study was carried out in triplicate (n = 3). After dipping BEADS in a desired fluid, each sample was kept under wild mechanical stirring (50 rpm), at 37 °C. At a desired time interval, an aliquot (3.0 mL) was removed from the flask to quantify de amount of released CUR through UV-Vis measures, as described above.

3. Results and discussion

3.1. Characterization of TMC by ^{1}H NMR

The differences in the ^{1}H NMR spectra showed in Fig. 1 inform that two different TMC (TMC20 and TMC80) were actually obtained. The DQ of each TMC was obtained from Eqs. (1) and (2), employing the areas of signals on ^{1}H NMR spectrum of TMC assigned to hydrogen atoms, as referred to in Section 2.3.1. The spectrum of CHT (Fig. 1a) shows signals at 1.90 ppm, referring to the methyl hydrogen atoms of the acetamide groups; at 2.96 ppm (H2); at 3.53–3.70 ppm (H3-H6); and at 4.69 ppm (H1), respectively. All these signals were assigned to hydrogen atoms present in the saccharide units of CHT [36].

Sieval et al. [32] obtained TMC with DQ of 60 mol% and they attributed the signal at 2.60 ppm to hydrogen atoms of N-monomethylated ($NHCH_3$) and N-dimethylated groups [$N(CH_3)_2$], labeled as NM and ND sites (Fig. 1). Sieval et al. [32] verified that the signal of the hydrogen atoms of NM and ND sites shifted to 3.10 ppm after adding a drop of DCl in the TMC solution, before proceeding ^{1}H NMR analyses. Therefore, the final pH of obtaining the TMC severely influences on chemical shift (δ) of the hydrogen atoms assigned to the NM and ND sites. It is known that the reaction for obtaining the TMC, described in Section 2.2.1, proceeds with the consumption of hydroxide ions. The values of δ in which the signals of methyl hydrogen atoms, of NM and ND sites, appear

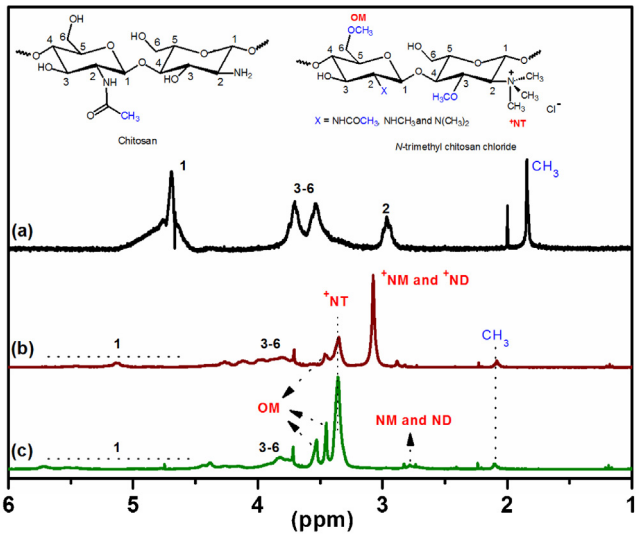

Fig. 1. ^{1}H NMR spectra of CHT (a), TMC20 (b) and TMC80 (c).

are dependent on reaction conditions, for instance on the final concentration of hydroxide ions [3,15,36].

Therefore, the ^{1}H NMR spectrum of TMC80 presented a peak of low intensity in the region of 2.70 ppm, attributed to the methyl hydrogen atoms of NM and ND sites (Fig. 1c). The low intensity of this peak was due to the high level of methylation on TMC80 (DQ = 80 mol%). This fact proves that the TMC80 has, in aqueous solution, non-charged NM and ND sites, because the signal of methyl hydrogen atoms appears precisely at 2.70 ppm. The excess of sodium hydroxide utilized in the synthesis of TMC80 (two-stepped method) keeps alkaline the reaction medium. Therefore, the signal of hydrogen atoms of methyl groups (NM and ND sites) occurs at 2.70 ppm (Fig. 1c). So, in an aqueous solution of TMC80 the NM and ND sites are in non-charged forms.

The signal related to the methyl hydrogen atoms of NM and ND sites in TMC20 absorbs exactly at 3.10 ppm (Fig. 1b) [32]. This fact indicates that the NM and ND sites in TMC20 are positively charged, according to the reactions $NM + H_3O^+ \rightarrow {}^+NM + H_2O$ and $ND + H_3O^+ \rightarrow {}^+ND + H_2O$. In this case the sodium hydroxide was not used in excess and the pH of the reaction medium decreases considerably during the course of reduction reaction (one-stepped method) influencing the δ of signal attributed to methylic hydrogen atoms present on NM and ND sites of TMC20 (Fig. 1b). The elevated consumption of hydroxyl ions in the one-stepped reaction decreased the pH to 4 and allowed the signal of hydrogen atoms of methylic groups ($^+$NM and $^+$ND sites) of TMC20 to appear at 3.10 ppm. Thus, the NM and ND sites of TMC20 are in charged forms, as $^+$NM and $^+$ND, respectively as in aqueous media. The signal at 3.35 ppm in the spectra (Fig. 1b and c) was due to the hydrogen atoms of the N-trimethylated groups [$^+N(CH_3)_3$], labeled as $^+$NT sites [32,37].

The signals at 3.45 and 3.55 ppm were assigned to the O-methylation in C3-OH and C6-OH (OM sites) and the signals attributed to hydrogen atoms H1 (Fig. 1b and c) occur at 4.7–5.7 ppm range [37]. The signal of H2 in ^{1}H NMR TMC spectra (Fig. 1b and c) is still unknown. Some authors have claimed that the H2 signal overlaps the signal attributed to hydrogen atoms of NM and ND sites [34,36]. The quaternization process also affects the δ value of the hydrogen atoms of acetamide groups (Fig. 1b and c).

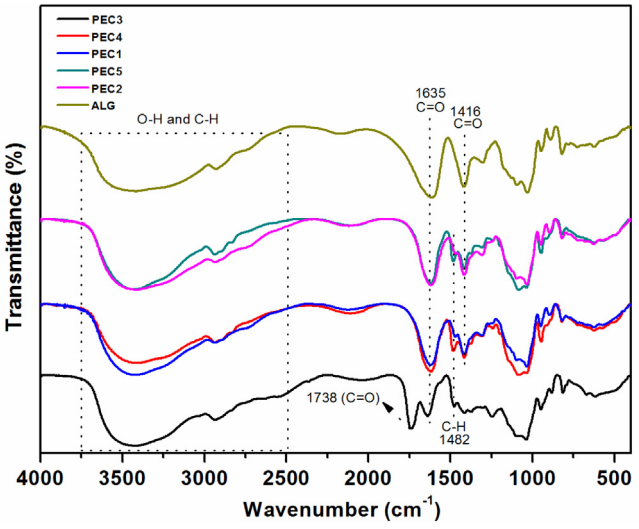

Fig. 2. FTIR spectra of PECs and pure ALG.

3.2. Intrinsic viscosity of TMC20 and TMC80 and their molecular weights

The greater number of steps employed in the synthesis of TMC favors increase of DQ [38] but provokes a decrease in molecular weight [39]. The TMC20 was obtained using one step methodology and presented M_V of 26×10^3 g mol^{-1}, while the TMC80 was prepared using two steps and presented M_V of 13×10^3 g mol^{-1}. Therefore, as expected, the methodology utilized for synthesis of TMC directly influences the average molecular weight of final product [39]. The excess of sodium hydroxide employing in synthesis of TMC80 considerably decreases the average molecular weight of CHT-derivative (TMC80) to 13×10^3 g mol^{-1}. Additionally, the lowest concentration of hydroxide ions employed in one step synthesis (TMC20) related to the two-stepped one, decreased the average molecular weight of CHT-derivative (TMC20) to 26×10^3 g mol^{-1}. The elevated concentration of hydroxide ions allows the cleavage of the glycosidic bonds and decreases the average molecular weight of TMC in relation to pure CHT [38–40]. According to Verheul et al. [40] the alkylation reaction condition of primary amines of CHT by reaction of this polymer in strong alkaline conditions with an excess of iodomethane and using NMP, as solvent, provides the scission of polymer chains and, importantly, partial and uncontrolled methylation of the C3 and C6 hydroxyl groups (OM sites) of CHT chains (Fig. 1).

Therefore, the average molecular weight of TMC decreased with the increase in the DQ. The increase in the DQ is determined by specific reaction time that leads to a decrease in the molecular weight of TMC polymers. It should be noted that the molecular weight of the polymer chain increases during the reductive methylation process, due to addition of methyl groups in the CHT chains. However, the observed decrease in the molecular weight is due to degradation of the polymer chains caused by exposure to the specific reaction conditions [38,39]. According to Hamman and Kotzé [39] the high number of reaction steps resulted in decrease of intrinsic viscosity of TMC solution, indicating that the molecular weight decreased with increased exposure time to the reaction conditions during the synthesis procedure. Thus, the intrinsic viscosity of TMC80 solution was lower as compared to the intrinsic viscosity of TMC20 solution (Fig. S1).

3.3. Characterization of PECs by FTIR spectroscopy

Fig. 2 shows the FTIR spectra of the ALG and PECs of TMC20/ALG (PEC1, PEC2) and TMC80/ALG (PEC3, PEC4 and PEC5). The band at 1482 cm^{-1} was attributed to the angular deformation of C—H bonds of methyl groups existing in TMC structure [15,16,41]. The wide band in the range from 2500 to 3750 cm^{-1} in spectra of FTIR was

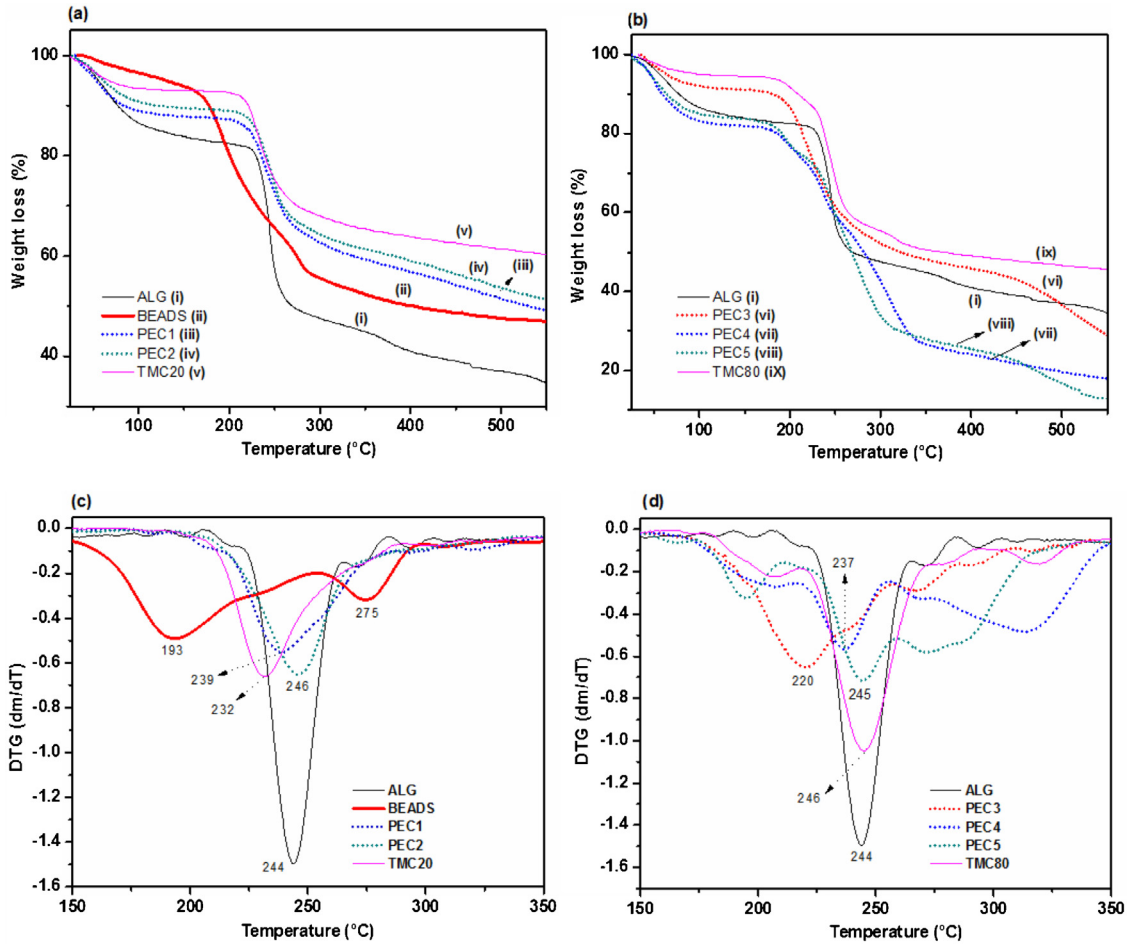

Fig. 3. TGA curves of TMC/ALG PECs formed at different pH conditions and the PEC-forming materials TMC20, TMC80 and ALG. (a) Using ALG and TMC20 and (b) using ALG and TMC80. First derivative (DTG) from TGA curves of raw materials ALG and TMC20 and TMC20/ALG PECs (c), ALG and TMC80 and TMC80/ALG PECs (d).

assigned to the characteristic stretches of C—H and O—H bonds and can be observed in all spectra showed in Fig. 2.

The band at 1635 cm^{-1} in the FTIR spectra of PECs was attributed to C═O bonds of secondary amide groups referred to the acetylated residues, that remain in the structure of TMC after the reduction reaction of CHT, and to the axial asymmetric deformation of carboxylate anions (Fig. 2) [15]. The bands that appear at 1416 cm^{-1} were assigned to axial symmetric deformation of carboxylate anions [41]. The spectrum of PEC3 presented a band at 1738 cm^{-1} attributed to C═O bonds of carboxylic groups (Fig. 2). The FTIR spectrum of BEADS was acquired using KBr (at 1.0 wt%) disc but the resolution was very bad (Fig. S2).

3.4. Characterization of PECs by TGA/DTG analysis

The TGA curves of different PECs and precursors (TMC20, TMC80 and ALG) are shown in Fig. 3a and b and the respective DTG curves are presented in Fig. 3c and d. The first stage of weight loss, attributed to the water evaporation, was observed in all TGA curves in 25–120 °C range. It should be important to notice that those samples showed different contents of water. The PEC precursors TMC20, TMC80 and ALG presented 6.6, 4.7 and 14.6 wt% of water content, respectively. The BEADS had the lowest water content, only 4.4 wt%, while the PEC3 presented 8.7 wt%. The PEC1, PEC2, PEC4 and PEC5 obtained on neutral or alkaline conditions possess water content of 11.7, 10.1, 17.7 and 15.8 wt%, respectively. At pH 2, the NM, ND and NH_2 sites of TMC are positively charged ($^+$NM, $^+$ND and $^+NH_3$). So, at pH 2 the $^+NH_3$, $^+$NM, $^+$ND and $^+$NT sites interact with the groups -COOH of ALG through of ion-dipole forces. TMC is a cationic polymer and presents good solubility in water due the quaternization of nitrogen atoms. However, as available in large extent in TMC, the methylic groups can provide hydrophobic characteristic in this polymer [15]. This property depends, obviously on the DQ and on molecular weight of TMC. Additionally, the low proportion of ionized carboxylic groups in the ALG structure decreases the affinity by water molecules at pH 2. This explains the low water contents on PEC3 and BEADS related to PEC1, PEC2, PEC4 and PEC5.

In neutral or alkaline conditions the carboxylic groups (—COOH) of ALG are fully ionized [42]. Therefore, the water molecules better interact with the ionized chains (ALG) through ion-dipole forces. In TMC these interactions occur in a lesser extent due to its hydrophobic character. This explains the higher water content on ALG as compared to TMC20 and TMC80 (Fig. 3a). So, the increase in water contents of PECs obtained in neutral or alkaline conditions depends on ionization process of carboxylic groups present in structure of ALG [42]. TGA/DTG analysis was processed immediately after obtaining the materials as described in Section 2.2.2. The drying process probably affected the water content of the samples, since the materials were subjected different drying processes.

The mass loss events related to degradation of the samples occur in the range from 150 to 350 °C, as showed in Fig. 3a and b. The TMC20, ALG and PECs of TMC20/ALG (PEC1 and PEC2) had only one event related to thermal degradation, while the BEADS presented three events of weight loss, being the two most pronounced of them occurred at 193 and 275 °C (Fig. 3a and c). This fact was expected

because the formation of BEADS occurred only at pH 2 as the TMC20 is used as polycation. Under these conditions, the NH_2, NM and the ND sites of TMC20 are mostly protonated and positively charged as $^{+}NH_3$, $^{+}$NM and $^{+}$ND, respectively. These sites interact with carboxylic groups of ALG molecules at pH 2, through ion-dipole forces. Therefore, the event at 193 °C can be attributed the rupture of the ion-dipole forces present on BEADS. The weight loss events at above 240 °C in the TGA curve of BEADS occur, probably, due the break of electrostatic interactions involving carboxylate anions of ALG and positively charged sites of TMC20. On the other hand, on alkaline conditions only the carboxylate groups and $^{+}$NT sites should be evolved in interactions to formation of PECs. This explains the differences on profile of TGA/DTG curves shown in Fig. 3a and c.

The degradation temperatures of TMC20, ALG, PEC1 and PEC2 occur at 232, 244, 239 and 246 °C, respectively, as determined by inflection of curves presented in Fig. 3c. The increase of pH favors obtaining more thermal stable PECs (TMC20/ALG). Martins et al., [15,16] obtained PECs of TMC/Heparin at pHs 10 and 12 with high thermal stability and each TGA/DTG curve from those PECs showed only one degradation event. However, the TMC80 and PECs of TMC80/ALG presented two or more thermal degradation events and they fall in the range of 150 to 350 °C (Fig. 3b and d). This fact can be associated to the high structural heterogeneity of TMC80. The degradation events on DTG curves presented maximum at 246, 220, 237 and 245 °C, respectively, for TMC80, PEC3, PEC4 and PEC5 (Fig. 3d). The temperatures in which the inflection points occur become higher as the pH of PEC-forming solution is increased. The profile of TGA/DTG curve of BEADS significantly differs of the others TGA/DTG curves of PECs. The PECs of TMC20/ALG presented higher thermal stability related to the PECs of TMC80/ALG, since the amount of residues at 550 °C for BEADS, PEC1 and PEC2 exceeded 40 wt% (Fig. 3a), while the residues at 550 °C for PEC3, PEC4 and PEC5 were lower than 40 wt% (Fig. 3b).

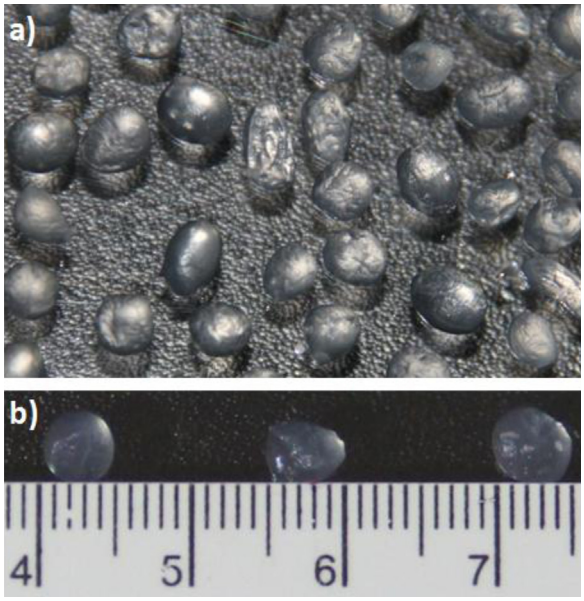

Fig. 4. Photographs of BEADS swollen.

3.5. Morphological analysis of BEADS

The Fig. 4 shows an image of the swollen BEADS. The BEADS presented diameter c.a. 0.50 cm even after being removed from the suspension with acetone (Fig. 4b). This separation process provides the diffusion out of water molecules and substantially reduces the size of swollen BEADS. The Fig. 5 shows SEM images of the dried BEADS at different magnifications. The average diameter of the dry samples was c.a. 0.10–0.20 mm. The morphology was dependent

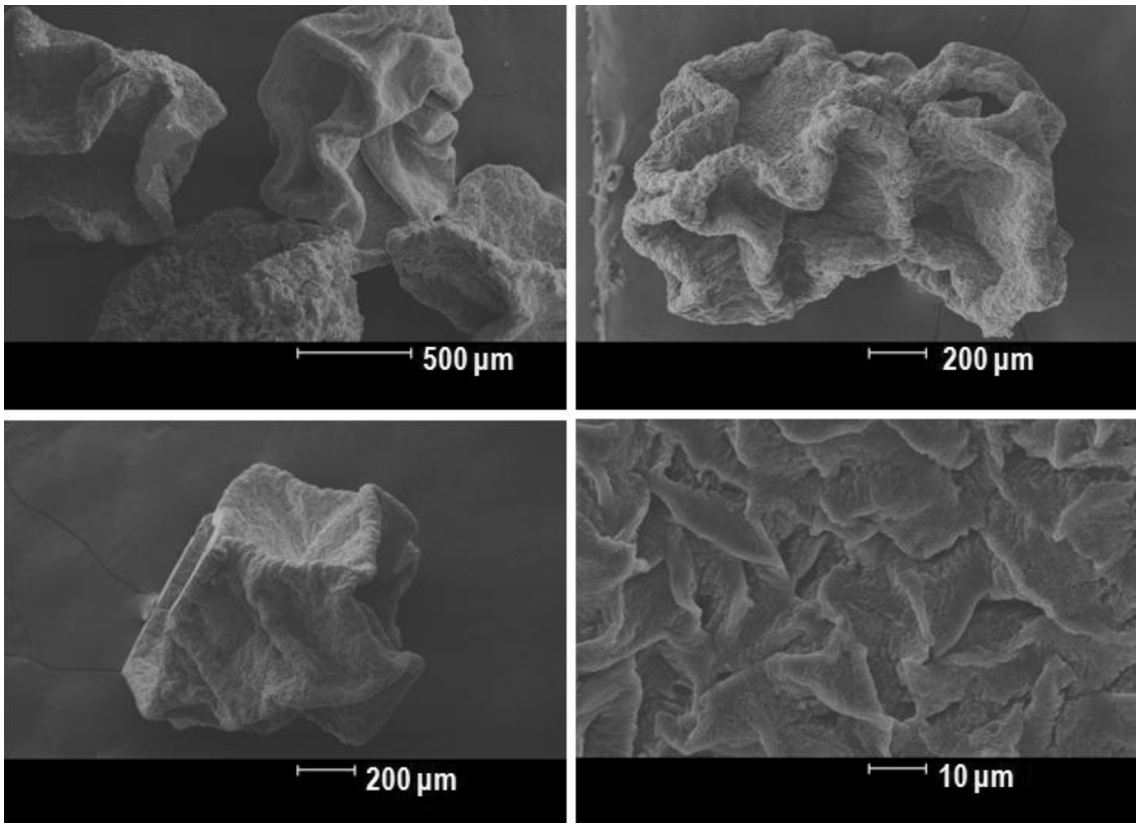

Fig. 5. SEM images of droughts BEADS with different magnifications.

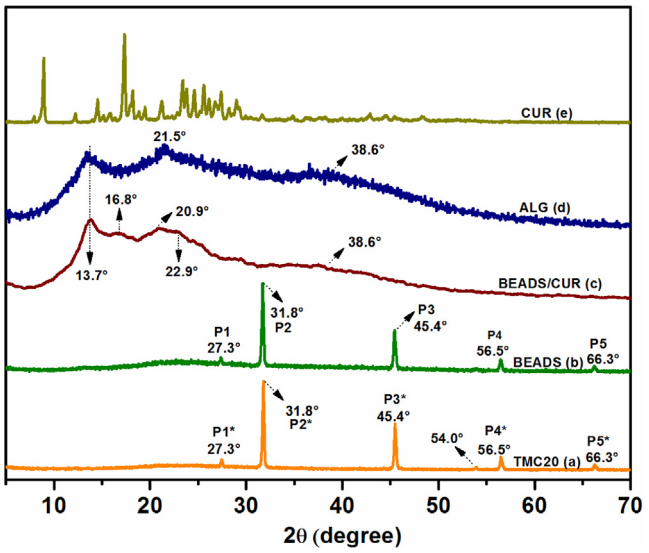

Fig. 6. WAXS profiles of the TMC20 (a), BEADS (b), BEADS/CUR (c), ALG (d) and CUR (e).

on the drying process, being possible to observe "folding" on the BEADS surface that hinder the pores of the materials (see the Fig. 5 of scale 10 μm).

The structure of CHT is characterized by the repeat units of β(1 → 4)-2-amine-2-deoxy-D-glycose. The amine group in repeat units of CHT show positive charges at pHs lesser than 6.5 [16]. ALG are anionic block copolymers of α-(1–4)-L-guluronic (G) and β-(1-4)-D-mannuronic acid (M). The pK_a values of M and G-residues are 3.38 and 3.65, respectively [42]. It is noteworthy that the BEADS were formed only in acidic medium. Therefore, the low DQ of TMC20, minimum proportion of ionized carboxyl groups in ALG chains and high density of positive charges in TMC structure at pH 2 were the key factors that led obtaining the BEADS.

In acidic medium (pH 2) the carboxylate groups of ALG are protonated, according to the reaction $-COO^- + H^+ \rightarrow -COOH$. Thus, the formation of BEADS occurs mainly due to the ion-dipole forces existing between the carboxylic groups of ALG molecules and $^+NH_3$, ^+NM, ^+ND and ^+NT sites of the TMC20. Therefore, the electrostatic interactions among the carboxylate groups ($-COO^-$) of ALG and positively charged sites of TMC20 occur with lower intensity at pH 2. On the other hand, the formation of TMC/ALG BEADS as the TMC80 is used does not occur in any pH, probably due to the high DQ of TMC80, low availability of $^+NH_3$, ^+NM, ^+ND sites and, at alkaline conditions, to high proportion of ionized carboxylic groups in the structure of ALG.

In the alkaline conditions or close to (pH > 6.5) the NM, ND, NH_2 groups are deprotonated, according to the reactions $^+NM + {}^-OH \rightarrow NM + H_2O$; $^+ND + {}^-OH \rightarrow ND + H_2O$ and $^+NH_3 + {}^-OH \rightarrow NH_2 + H_2O$. These factors prevented formation of BEADS. So, the complexation of ALG and TMC at neutral or alkaline conditions occurs primarily with the ^+NT quaternized sites of TMC and $-COO^-$ groups of ALG. The greater effectiveness of the electrostatic interactions among ^+NT and $-COO^-$ groups at alkaline conditions enables obtaining PECs in precipitate form [15,16].

3.6. WAXS analysis

Fig. 6 shows the WAXS profiles of TMC20, BEADS, ALG, BEADS/CUR and pure CUR. The WAXS profile of TMC20 salt (curve a) exhibits well defined diffraction peaks at 2θ = 27.3, 31.8, 45.4, 54.0, 56.5 and 66.3° [16].

Table 1
Areas of diffraction peaks at 2θ = 27.3° (P_1), 31.8° (P_2), 45.4° (P_3), 56.5° (P_4) and 66.3 (P_5), together with the ratios P_2/P_x, P_3/P_x, P_{2^*}/P_{1x^*} and P_{3^*}/P_{x^*} observed on TMC20 and BEADS WAXS profiles (diffractogram shown in Fig. 6). The (*) means the data from WAXS of TMC20.

	Diffraction peak areas (a.u.)				
2θ	27.3°	31.8°	45.4°	56.5°	66.3°
P*	0.0388	0.226	0.140	0.0463	0.0208
P	0.454	0.954	0.899	0.629	0.585
P_2/P_x	2.1	1	1.1	1.5	1.6
P_3/P_x	2.0	0.94	1	1.4	1.5
P_{2^*}/P_{x^*}	5.8	1	1.6	4.9	10.8
P_{3^*}/P_{x^*}	3.6	0.62	1	3.0	6.7

The WAXS profile of BEADS (curve b) shows the same diffraction peaks observed in WAXS profile of TMC20. To better analyzing the complexation influences on crystalline regions of BEADS, the areas of diffraction peaks observed in the WAXS profiles of Fig. 6 (curves a-b) were evaluated. Thus, the area ratios P_2/P_1, P_2/P_2, P_2/P_3, P_2/P_4 and P_2/P_5 were calculated from the WAXS profile of BEADS and labeled as P_2/P_x. Similarly, the area ratios P_3/P_1, P_3/P_2, P_3/P_3, P_3/P_4 and P_3/P_5 were calculated from the WAXS profile of BEADS and labeled as P_3/P_x. The same procedure was adopted for the peaks on WAXS profile of TMC20 (curve a) and the ratios were labeled as P_2^*/P_x^* and P_3^*/P_x^*. The results are shown in the Table 1. It was found that the ratios P_2/P_x, in general, are lower than the ratios P_2^*/P_x^*. The same fact occurs when the ratios P_3/P_x are compared to P_3^*/P_x^* being $P_3/P_x < P_3^*/P_x^*$ for all cases. The areas of P_2, P_2^*, P_3 and P_3^* are mainly related to the crystalline arrangement provided by the interaction of chloride ions with the oppositely charge ions (^+NT) of TMC20 [16]. Therefore, being the $P_2^*/P_x^*$and P_3^*/P_x^* area ratios on WAXS profile of raw TMC20 higher than those on WAXS profile of TMC20 on BEADS, it allows to infer that the crystallinity of TMC20 segments is substantially reduced on BEADS. The interactions existing between TMC20 and ALG disturb the interactions among chloride ions and ^+NT sites and led to decrease the crystallinity of TMC20 on BEADS (curve b) as compared to neat TMC20 salts (curve a).

The real effect of CUR-loading process on the BEADS structure was explained from the analysis of the schema presented in Fig. 7 and through of the differences observed in the WAXS profiles of BEADS and BEADS/CUR (Fig. 6). The Fig. 7a shows the basic saccharide units of the TMC iodide, TMC chloride and TMC hydroxide. Xu et al. [43] and Follmann et al. [33] related that the exchange of the chloride ions by hydroxyl anions in the N-trimethylated sites (^+NT), from aqueous TMC-solution, is favored at pH > 5.5, according to the Equations

$$-NT^+Cl^- \leftrightarrow {}^+NT + Cl^- \quad (3)$$

$$-{}^+NT + H_2O \leftrightarrow NT^+OH^- + H^+ \quad (4)$$

According to Xu et al. [43] the $-NT^+Cl^-$ groups could not interact with the negative charged sites on cell envelope of *Escherichia coli* (*E. coli*) and TMC95 (TMC with DQ = 95 mol%) presented strong bactericidal activity only at pH > 5.5. Follmann et al. [33] developed thin films of TMC80/Heparin (TMC80/HP) and evaluated the biocide action of the TMC80/HP system against *E. coli* at pH 7.4. According to Follmann et al. [33] TMC80/HP assembled at pH 3.0 showed low antibacterial activities, since that the $-NT^+Cl^-$ sites are not initially dissociated. So, the chains of TMC80 at pH 3.0 are not flexible enough to interact with the *E. coli* cell envelope. On the other hand, the TMC80/HP system assembled at pH 7.4 showed high bactericidal action, because at this pH-condition the $-NT^+Cl^-$ sites are initially dissociated, providing enough mobility the chains of TMC80 [33]. Therefore, Xu et al. [43] and Follmann et al. [33] showed through independent works that the TMC chloride can

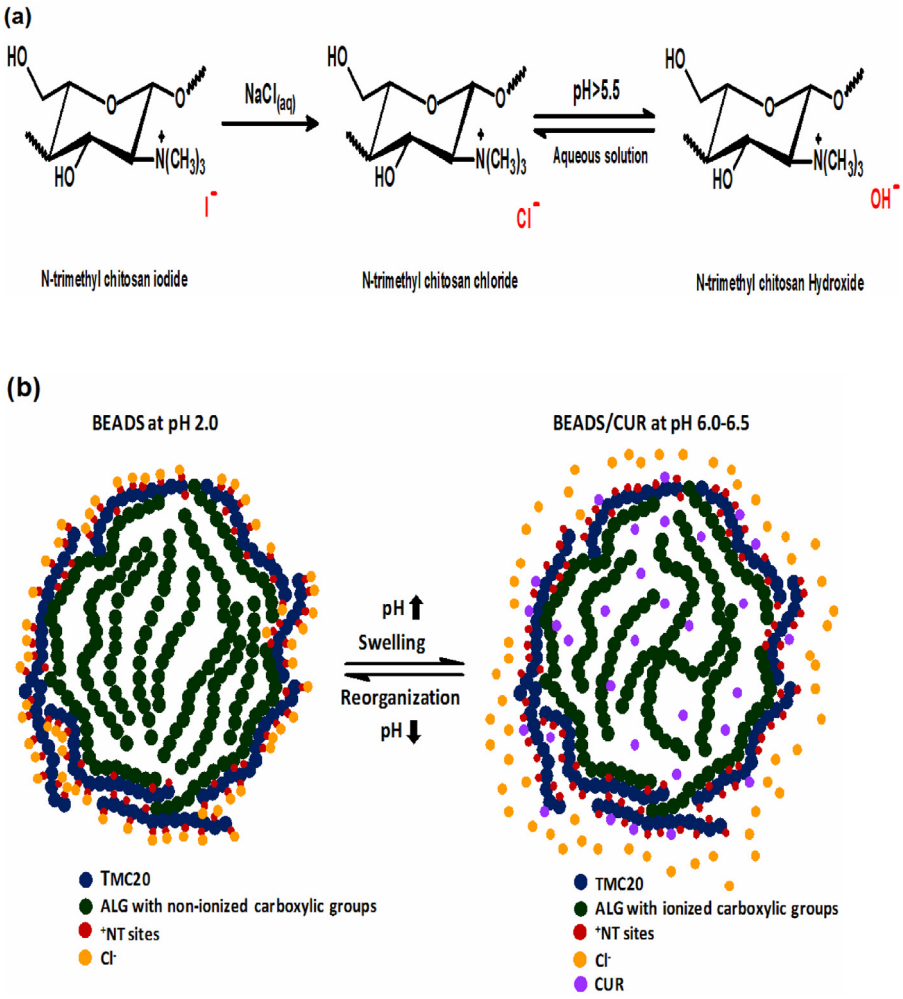

Fig. 7. (a) Structure of the TMC salts (iodide, chloride and hydroxide). (b) Physical structure of dried BEADS at pH 2 (left side) and BEADS-loaded with CUR at pH 6.0–6.5 (right side), depicting the shielding and dissociation processes that occur in the $NT^{+}Cl^{-}$ groups present in the BEADS surface.

dissociate in aqueous solutions (pH > 5.5). However, these effects no were verified by techniques as for example WAXS and DSC analysis.

So, significant differences between the WAXS profiles of BEADS (curve b) and BEADS/CUR (curve c) were observed. The BEADS were formed at acid conditions from HCl aqueous solution at pH 2. This condition favors the association among TMC20 and ALG molecules and also provided an effective shielding on the $^{+}$NT groups, present in BEADS surface (Fig. 7b left side). The shielding of positively charged TMC20 sites in BEADS structure is provided by the presence of chloride ions. According to Xu et al. [43] and Follmann et al. [33] the shielding of N-trimethylated charged sites ($^{+}$NT) in TMC chains is more pronounced at low pHs and disadvantaged at pHs > 5.5 (see Fig. 7a). Therefore, the occurrence of effective interactions among chloride ions and $^{+}$NT sites present in the BEADS surface at pH 2 was inferred by the appearance of same diffraction peaks at $2\theta = 27.3$, 31.8, 45.4, 56.5 and 66.3° in WAXS profile of TMC20 salt (curve a) [16].

On the other hand, once the CUR is incorporated into BEADS at pH 6.0–6.5 this condition favors, initially, the dissociation [43] of TMC20 chloride present in BEADS surface, and also then the deprotonation of $^{+}NH_3$, $^{+}$NM, $^{+}$ND and —COOH groups that are pH-dependent. In scheme of Fig. 7b (right side) the ALG molecules are in the ionized form and the swelling of BEADS is favored, whereas the reorganization process is disadvantaged. Thus, the encapsulation process of CUR at pH 6.0–6.5 afforded the change in WAXS profile of BEADS/CUR related to the WAXS profile of unloaded BEADS. The absence of diffraction peaks at $2\theta = 27.3$, 31.8, 45.4, 56.5 and 66.3° in WAXS profile of BEADS/CUR (curve c) confirms this fact. The appearance of broad peaks at $2\theta = 13.7$, 16.8, 20.9, 22.9 and 38.6° in WAXS profile of BEADS/CUR indicates the presence of crystalline domains on BEADS/CUR structure. These crystalline domains were attributed to ordered regions formed by intra and intermolecular interactions among ALG-ALG, TMC20-ALG and TMC20-TMC20 chains segments. It should be noticed that the WAXS profile of BEADS/CUR (curve c) is similar to the WAXS profile of pure ALG (curve d), since the same broad diffraction peaks of low intensity in the range at $2\theta = 13.7$, 21.5 and 38.6° occurs in both diffractograms (curves c–d of Fig. 6). This fact characterizes the low crystallinity of BEADS/CUR (curve c) related to unloaded BEADS (curve b).

The WAXS profile of CUR (curve e) showed diffraction peaks in the 2θ range of 10 to 30° implying its crystalline nature, but in WAXS profile of BEADS/CUR (curve c) there were no such crystalline peaks. So, in contrast to its crystalline arrangement as in pure form, the CUR comprises an amorphous or disordered-crystalline phase as encapsulated in the BEADS. This also indicate that the CUR is well dispersed in the BEADS slowing its degradation, increasing the bioactivity and enabling possible application of the BEADS in area of controlled drug delivery.

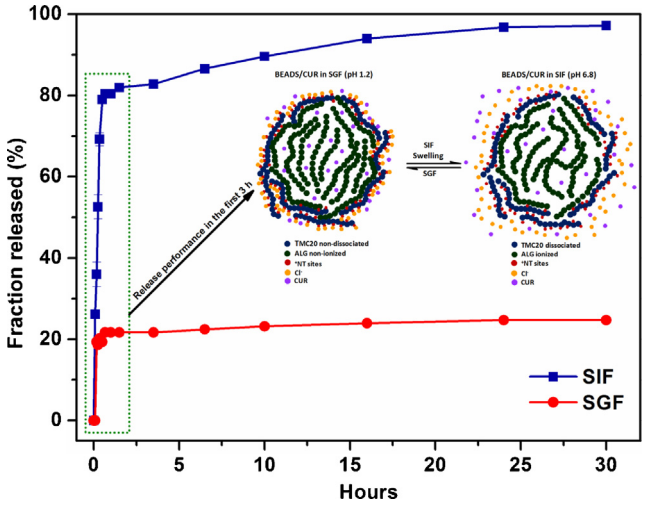

Fig. 8. Fraction released (%) of CUR from BEADS in SIF and SGF, depicting the swelling of PEC and the diffusion process of CUR in SIF in the first 3 h.

3.7. Thermal analysis

Figure S3 (supplementary information) shows DSC curves of BEADS/CUR, CUR and pure BEADS. The DSC curve of CUR presented a strong endothermic peak at 179 °C that was due to crystalline nature of CUR, whereas the DSC curve of BEADS/CUR displayed no pronounced peak in this same region. The DSC curves of BEADS and BEADS/CUR have other stronger differences that were related to the shielding effect on $^{+}$NT sites of TMC20 at BEADS surface (Fig. 7b, left side) and also to the dissociation and deprotonation processes that occur on interface of BEADS/CUR at pH 6.0–6.5 (Fig. 7b, right side). This result is in agreement with the WAXS data and allowed to infer that the CUR comprises disordered phase in the BEADS structure. Anitha et al. [44] prepared dextran sulphate-chitosan nanoparticles (NPs) loaded with CUR. From the DTA and WAXS techniques, Anitha and co-workers showed that CUR comprises an amorphous phase encapsulated in the NPs structure. Therefore, the results presented in this study are consistent with data published by Anitha et al. [44].

3.8. In vitro curcumin release from BEADS

Recent studies confirm the efficacy of CUR against several types of cancers, such as prostate cancer, bone cancer, head and neck cancer, lung cancer and gastrointestinal cancer. The CUR still has a wide range of pharmacological applications such as anti-inflammation, anti-human immune-deficiency virus, anti-microbial, anti-oxidant and anti-parasitic. However, in spite of this wide spectrum of pharmacological properties, the application of CUR in clinic has been hampered due to low solubility in aqueous solution (c.a. 11 ng mL^{-1} in aqueous buffer solution, at pH 5) and rapid degradation at physiological pH. The absorption process of CUR in gastro-intestinal tract is very low, for example, the absolute oral bioavailability in rat is only about 1.0% [26–30]. All these factors hinder the application of this drug in the fighting against the cancer. As a tentative for overcoming this restriction, the BEADS were applied as protective matrix of CUR and the *in vitro* release of the drug in simulated environments were evaluated. Fig. 8 shows the fraction of CUR released from the BEADS as immersed in SGF or SIF.

According to results, the efficiency of loading CUR into the BEADS was 82%, indicating that 0.82 mg of CUR was loaded in 1.0 g of BEADS. According to Fig. 8, in the first hour, c.a. 80% of loaded CUR was released in SIF. On the other hand, in this same time interval the fraction of CUR released in SGF was only 21.6%. In the first 15 min a burst release of CUR was observed in both cases (19.4% in SGF and 36.0 in SIF). So, the CUR that is adsorbed at the BEADS surface or entrapped near the interface might be the reason for the initial burst release. According to Anitha et al. [44] the dissolution rate of the polymers (dextran sulphate and CHT) near the surface of the dextran sulphate-chitosan nanoparticles is high and the amount of released CUR was also high. Therefore, the ionization of the carboxylic groups of ALG, favors the swelling of BEADS (see Fig. 7b). Consequently the release of adsorbed or entrapped CUR near the BEADS surface was c.a. 80% in SIF during the first hour of release test. The low crystallinity of CUR dispersed on the BEADS can favor the rapid drug release and the increase the bioactivity of CUR. The equilibrium was achieved within 24 h of study in SIF and within 45 min in SGF. Moreover, about 100% of CUR was released in SIF up to 24 h against c.a. 30% in SGF, in same period. These results enable the potential applications of BEADS as carrier of CUR in the gastrointestinal tract.

The largest fraction of CUR released in SIF compared to SGF occurs due to the ionization process of —COOH groups at pH 6.8, according to the reaction $—COOH + H_2O \rightarrow —COO^- + H_3O^+$. This fact promotes stronger interactions among carboxylate groups of ALG chains and water molecules, leading to swelling of the BEADS. Thus, the release mechanism of CUR from the BEADS in SIF is more related to drug diffusion and swelling processes. In SGF (pH 1.2) the —COO$^-$ groups are protonated, remaining as —COOH. At pH 1.2 the $^{+}$NM, $^{+}$ND and $^{+}$NT groups interact with —COOH groups through of ion-dipole forces, preventing the association with water molecules and the swelling of BEADS in SGF. The hydrophobic characteristic of TMC sites ($^{+}$NM, $^{+}$ND and $^{+}$NT) and lack of dissociation of TMC molecules in SGF also hinders the association with water molecules at pH 1.2 [16]. Thus, the fraction of CUR released in SGF is 3.3 times lower than the fraction released in SIF. The illustration inserted in Fig. 8 shows the release performance of CUR from BEADS in the first 3 h, depicting the swelling of PEC and the diffusion process of CUR in SIF. The BEADS did not suffer fragmentation during the release tests.

Many formulation strategies including micelles, liposomes, microspheres, beads and solid lipid particles have already been explored to design delivery systems of CUR [45,46]. According to Chen et al. [45] the CUR incorporated into TMC-coated liposomes exhibited different pharmacokinetic parameters and enhanced bioavailability, compared to the CUR encapsulated by uncoated liposomes and CUR suspension. Therefore, the oral delivery of CUR from the TMC-coated liposomes is a promising strategy for poorly water-soluble CUR [45]. Song and co-workers [46] developed curcumin-loaded alginate beads through physical gelification with Ca^{2+} ions, containing different emulsifiers (Span-80 and Tween-80). The studies showed that almost all of the CUR-loaded in the beads was released (buffer solution at pH 7.2) within about 20 h and the release rates could be regulated by changing the Tween-80 and Span-80 concentrations [45]. Therefore, Song et al. [46] and Chen et al. [45] in independent works, showed that the materials based on ALG (beads) and TMC (TMC-coated liposomes) may be used as potential carriers to improve the solubility and stability of CUR at physiological pH.

In this work, the system composed by TMC20 and ALG formed BEADS at pH 2.0. Therefore, it could be concluded from the results showed in Fig. 8 that the BEADS of TMC20/ALG might serve as a potential carrier, because it improved the biological activity of CUR close to the physiological pH. As mentioned above the TMC and the ALG, individually, allowed excellent properties to the materials developed by Chen et al. [45] and Song et al. [46]. However, this paper described, by the first time, the BEADS formation as an association between the TMC and ALG polysaccharides. The BEADS are constituted by water-soluble polymers that have low toxicity and are biocompatible and biodegradable [5,22,23]. Such properties can

Table 2
Values of diffusional exponent (n) and constant (k) obtained by application of Ritger–Peppas model (Eq. (5)) in mediums with different pHs, at 37 °C.

pH	n	k	R^2
pH 6.8 (SIF)	0.66	1.34	0.96
pH 1.2 (SGF)	0.042	0.85	0.97

potentiate future applications of the BEADS as protective matrix of CUR at physiological pH.

3.9. Transport mechanism of CUR from BEADS matrix

The release process can occurs as a diffusional transport process and/or as a partition phenomenon in which the partitioning of solutes between the solvent phase and the hydrogel takes place. Ritger and Peppas [47] proposed a well know semi-empirical model that describes the mechanism related to transport of solutes from a flexible matrix that is given by the equation

$$\frac{M_t}{M_\infty} = kt^n \quad (5)$$

where M_t and M_∞ represent the amount of solute released at time t and at equilibrium, respectively, being the M_t/M_∞ is the fractional drug released, k is a constant dependent on the solvent/polymer and external conditions (like pH, temperature, ionic strength, *etc.*) and n is the diffusional exponent that can be related to the drug transport mechanism [47]. The Eq. (5) characterizes the solvent diffusion mechanism within the gel or the release mechanism of the solute. When n is around 0.5, the drug release mechanism would be controlled by Fickian diffusion [48]. For $n = 1$, the transport mechanism is described for a kinetics of zero order. In this case, the amount of released solute increases straightforward with time. This fact is associated to the macromolecular relaxation of polymeric chains of the hydrogel matrix. When the value of n is between 0.5 and 1.0, an anomalous transport is observed, which result of simultaneous contributions of diffusion and matrix relaxation [48].

The values of n and k for were obtained from releasing curves (Fig. 8) using Eq. (5) and are presented in (see Table 2). The value of n was 0.66 for SIF. According to Ritger and Peppas [47,48] release systems have a spherical geometry presented n value between 0.5 and 1.0. So, the results described in this work are according with the date reported by Ritger and Peppas [48]. Therefore, the amount of CUR released from BEADS matrix in SIF middle was a contribution of the diffusion process and hydrogel matrix relaxation, which characterize an anomalous transport. This fact confirms that CUR released in SIF is related with swelling process, whereas both the processes of diffusion and macromolecular relaxation are related with the BEADS swelling in SIF. On the other hand, n value for SGF was 0.042. This lower value characterizes the weak affinity of BEADS for water molecules. At pH 1.2 (SGF) the BEADS do not swell as at pH 6.8 (SIF). So, the fraction of CUR released in SGF was lower as compared to the fraction released in SIF. In this case, the diffusion of water molecules into the hydrogel matrix do not occurs, which must inhibit or minimizes the chain relaxation. Therefore, the fraction of CUR released in SGF is closely related to the amount of drug adsorbed on the surface of the BEADS. According to Ritger and Peppas [47] k is a constant dependent on solvent/polymer system. Thus, the values obtained showed that BEADS exhibited pH-sensitive property, with higher values of k in SIF (Table 2).

When the equilibrium is reached (Fig. 8), the release and absorption rates of CUR are equivalent and the fractional release (F_r) attain a maximum value (F_{max}) for a given condition. In this way, the CUR released from hydrogel could be treated as a diffusion phenomenon and/or partition phenomenon [49]. With F_{max} and F_r parameters obtained from the release curve performed in SIF (Fig. 8), the respective kinetic constant of release (k_r) could be determinate using the partition-diffusion mathematical model (Eq. (6)), assuming that release occurs according to first-order kinetics [49]. The value of rate constant for the CUR releasing (k_r) from the BEADS in SIF is presented in Table 3. The obtention of Eq. (6) is detailed in the work of Reis et al. [49] published elsewhere by our research group.

Table 3
Value of constant (k_r) obtained from the Eq. (6) in SIF at 37 °C.

pH	k_r	R^2
6.8 (SIF)	3.21	0.99

$$F_{max} \ln\left(\frac{F_{max}}{F_{max} - F_r}\right) = K_r T \quad (6)$$

According to Peppas et al. [47] the semi-empirical relation (Eq. (5)) is valid only for a certain time interval, *i.e.*, the time in which up to 60% of the initial amount of solute is released [47,48]. On the other hand, the model related to Eq. 6 can predict the entire release of solute, *i.e.* 100% [49]. From the analysis of Figure S4 (supplementary material) it can be seen as the models proposed by the Eqs. (5) and (6) if adjusted to the experimental data for the first 3 h of assay in SIF. The Figure S4 shows curves of F_r as a function of time in SIF. For comparison purposes, the curves obtained by application of Eqs. (5) and (6) were superimposed to experimental data obtained in SIF (Fig. 8). The data described by the Eq. (5) are in accordance with the experimental curve only in the first 1/2 h of release assay, where F_r reaches 0.6–0.7. On the other hand, the curve predicted by use of Eq. (6) is in good accordance with the experimental results exhibited in the release profile in SIF (Fig. S4). So, the release profile of CUR from BEADS can be adjusted by the first-order kinetic model. The high value of k_r (3.21) explains the rapid release of CUR in the first 3 h of assay.

4. Conclusions

N-trimethyl chitosan (TMC) were synthesized at two different degree of quaternization (DQ = 20 and 80 mol%). Polyelectrolyte complexes of each type of TMC and alginate (ALG) were obtained at pHs 2, 7 and 10 by mixing the aqueous solutions of unlike polymers. The materials were characterized by FTIR, WAXS, SEM and TGA/DTG analysis. Using the TMC of DQ 20 mol% (TMC20) and following the same methodology for preparing the PECs, BEADS of TMC20/ALG were obtained at pH 2. The BEADS presented the lower water content and lower thermal stability compared to the other PECs of TMC20 and TMC80 prepared in this work. Studies of controlled release of curcumin (CUR) were performed on different environments (SGF and SIF), employing the CUR-loaded BEADS as drug carrier. The results were satisfactory, since that c.a. 100% of loaded CUR was released on SIF after 24 h.

Acknowledgments

A.F.M. thanks to CNPq by doctorate's fellowship. A.F.R. and E.C.M. thank to CNPq by financial support (Proc. 481424/2010-5 and 309005/2009-4).

Appendix A. Supplementary data

Supplementary data associated with this article can be found, in the online version, at http://dx.doi.org/10.1016/j.ijbiomac.2013.03.029.

References

[1] A.F. Martins, D.M. Oliveira, A.G.B. Pereira, A.F. Rubira, E.C. Muniz, International Journal of Biological Macromolecules 51 (2012) 1127–1133.
[2] D-K. Kweon, S-B. Song, Y-Y. Park, Biomaterials 24 (2003) 1595–1601.
[3] V.K. Mourya, N.N. Inamdar, Journal of Materials Science–Materials in Medicine 20 (2009) 1057–1079.
[4] A.F. Kotze, M.M. Thanou, H.L. Luebetaen, A.G. De Boer, J.C. Verhoef, H.E.J. Junginger, Journal of Pharmaceutical Science 88 (1999) 253–257.
[5] S.M. Van der Merwe, J.C. Verhoef, J.H.M. Verheijden, European Journal of Pharmaceutics and Biopharmaceutics 58 (2004) 225–235.
[6] M. Thanou, J.C. Verhoef, H.E. Junginger, Advanced Drug Delivery Reviews 52 (2001) 117–126.
[7] A. Jintapattanakit, V.B. Junyaprasert, S. Mao, J. Sitterberg, U. Bakowsky, T. Kissel, International Journal of Pharmaceutics 342 (2007) 240–249.
[8] G. Di Colo, S. Burgalassi, Y. Zambito, D. Monti, P. Chetoni, Journal of Pharmaceutical Science 93 (2004) 2851–2862.
[9] B.C. Baudner, J.C. Verhoef, M.M. Giuliani, S. Peppoloni, R. Rappuoli, G. Del Giudice, H.E. Junginger, Journal of Drug Targeting 13 (2005) 489–498.
[10] G. Sandri, S. Rossi, M.C. Bonferoni, F. Ferrari, Y. Zambito, G. Di Colo, C. Caramella, International Journal of Pharmaceutics 297 (2005) 146–155.
[11] B.I. Florea, M. Thanou, H.E. Junginger, G. Borchard, Journal of Controlled Release 110 (2006) 353–361.
[12] W. He, Y. Du, W. Dai, Y. Wu, M. Zhang, Journal of Applied Polymer Science 99 (2006) 1140–1146.
[13] S. Warayuth, G. Pattarapond, R.U. Rungsardthong, International Journal of Biological Macromolecules 48 (2011) 589–595.
[14] S.K. Jasjeet, C. Shruti, A.J. Farhan, Journal Pharmacy and Pharmacology 60 (2008) 1111–1119.
[15] A.F. Martins, J.F. Piai, I.T.A. Schuquel, A.F. Rubira, E.C. Muniz, Colloid and Polymer Science 289 (2011) 1133–1144.
[16] A.F. Martins, A.G.B. Pereira, A.R. Fajardo, A.F. Rubira, E.C. Muniz, Carbohydrate Polymers 86 (2011) 1266–1272.
[17] B. Sayin, S. Somavarapu, X.W. Li, D. Sesardic, S. Senel, O.H. Alpar, European Journal Pharmaceutical Science 38 (2009) 362–369.
[18] L. Yin, J. Ding, C. He, L. Cui, C. Tang, C. Yin, Biomaterials 30 (2009) 5691–5700.
[19] S. Cafaggi, E. Russo, R. Stefani, R. Leardi, G. Caviglioli, B. Parodi, G. Bignardi, D. De Totero, C. Aiello, M. Viale, Journal of Controlled Release 121 (2007) 110–123.
[20] O. Germershaus, S. Mao, J. Sitterberg, U. Bakowsky, T. Kissel, Journal of Controlled Release 125 (2008) 145–154.
[21] B. Slutter, P.C. Soema, Z. Ding, R. Verheul, W. Hennink, W. Jiskoot, Journal of Controlled Release 143 (2010) 207–214.
[22] Z. Zhi-De, L. Gui-Yin, L. Yuan-Jian, International Journal of Biological Macromolecules 47 (2010) 21–26.
[23] S.M. Jay, W.M. Saltzman, Journal of Controlled Release 134 (2009) 26–34.
[24] H.F. Hassan, H.S. Ramaswamy, Journal Food Engineering 107 (2011) 117–126.
[25] J.S. Yang, H.B. Ren, Y.J. Xie, Biomacromolecules 12 (2011) 2982–2987.
[26] R.K. Basniwal, H.S. Buttar, V.K. Jain, N. Jain, Journal Agricultural and Food Chemistry 59 (2011) 2056–2061.
[27] R.K. Singh, D. Rai, D. Yadav, A. Bhargava, J. Balzarini, E. De Clercq, European Journal Medicinal Chemistry 45 (2010) 1078–1086.
[28] X. Qiu, Y. Du, B. Lou, Y. Zuo, W. Shao, Y. Huo, J. Huang, Y. Yu, B. Zhou, J. Du, H. Fu, X. Bu, Journal of Medicinal Chemistry 53 (2010) 8260–8273.
[29] N. Bhagavathula, L.R. Warner, M. DaSilva, S.D. McClintock, A. Barron, M.N. Aslam, K.J. Johnson, J. Varani, Wound Repair and Regeneration 17 (2009) 360–366.
[30] A. Barik, N. Praveen, K.I. Priyadarsini, National Academy Science Letters-India 28 (2005) 383–388.
[31] M.R. Guilherme, M.R. Moura, E. Radovanovic, G. Geuskens, A.F. Rubira, E.C. Muniz, Polymer 46 (2005) 2668–2674.
[32] A.B. Sieval, M.M. Thanou, A.F. Kotzé, J.C. Verhoef, J. Brussee, H.E. Junginger, Carbohydrate Polymers 36 (1998) 157–165.
[33] H.D. Follmann, A.F. Martins, A.P. Gerola, T.A.L. Burgo, C.V. Nakamura, A.F. Rubira, E.C. Muniz, Biomacromolecules 13 (2012) 3711–3722.
[34] E. Curti, P.S. Campana-Filho, Journal Macromolecular Science-pure and Applied Chemistry 43 (2006) 555–572.
[35] F. Atyabi, S. Majzoob, M. Iman, M. Salehi, F. Dorkoosh, Carbohydrate Polymers 61 (2005) 39–51.
[36] D. Britto, A.L. Forato, O.B.G. Assis, Carbohydrate Polymers 74 (2008) 86–91.
[37] J.H. Hamman, C.M. Schultz, A.F. Kotze, Drug Development and Industrial Pharmacy 29 (2003) 161–172.
[38] D. Snyman, J.H. Hamman, J.S. Kotze, J.E. Rollings, A.F. Kotzé, Carbohydrate Polymers 50 (2002) 145–150.
[39] J.H. Hamman, A.F. Kotzé, Drug Development and Industrial Pharmacy 27 (2001) 373–380.
[40] J.R. Verheul, M. Amidi, S. Van der Wal, E. Van Riet, W. Jiskoot, W.E. Hennink, Biomaterials 29 (2008) 3642–3649.
[41] F-L. Mi, Y-Y. Wu, Y-H. Lin, K. Sonaje, Y-C. Ho, C-T. Chen, J-H. Juang, H-W. Sung, Bioconjugate Chemistry 19 (2008) 1248–1255.
[42] X-X. Li, H-G. Xie, J-Z. Lin, W-Y. Xie, X-J. Ma, Polymer Degradability and Stability 94 (2009) 1–6.
[43] T. Xu, M. Xin, M. Li, H. Huang, S. Zhou, Carbohydrate Polymers 81 (2010) 931–936.
[44] A. Anitha, V.G. Deepagan, D.V.V. Rani, D. Menon, S.V. Nair, R. Jayakumar, Carbohydrate Polymers 84 (2011) 1158–1164.
[45] H. Chen, J. Wu, M. Sun, C. Guo, A. Yu, F. Cao, L. Zhao, Q. Tan, G. Zhai, Journal of Liposome Research 22 (2012) 100–109.
[46] S. Song, Z. Wang, Y. Qian, L. Zhang, L. Erfeng, Journal of Agricultural and Food Chemistry 60 (2012) 4388–4395.
[47] L. Serra, J. Doménech, N.A. Peppas, Biomaterials 27 (2006) 5440–5451.
[48] N.A. Peppas, J.J. Sahlin, International Journal of Pharmaceutics 57 (1989) 169–172.
[49] A.V. Reis, M.R. Guilherme, A.F. Rubira, E.C. Muniz, Journal Colloid and Interfaces Science 310 (2007) 128–135.